Fuel Processing Technology 213 (2021) 106672

Contents lists available at ScienceDirect

Fuel Processing Technology

journal homepage: www.elsevier.com/locate/fuproc

Research article

Catalytic hydrogenation and etherification of 5-Hydroxymethylfurfural into 2-(alkoxymethyl)-5-methylfuran and 2,5-bis(alkoxymethyl)furan as potential biofuel additives

Islam Elsayed [a,b], Michael A. Jackson [c], El Barbary Hassan [a,*,1]

[a] Department of Sustainable Bioproducts, Mississippi State University, Box 9820, Mississippi State, MS 39762, USA
[b] Department of Chemistry, Faculty of Science, Damietta University, New Damietta, Damietta Governorate 34517, Egypt
[c] United States Department of Agriculture, Agricultural Research Service, National Center for Agricultural Utilization Research, Renewable Products Technology Research, 1815 N. University St. Peoria, IL 61604, USA

ARTICLE INFO

Keywords:
HMF
Alkoxymethylfurans (AMFs)
2,5-Bis(alkoxymethyl)furans (BAMFs)
Catalytic transfer hydrogenation
Etherification
Biofuel additives

ABSTRACT

In this study, 5-hydroxymethylfurfural (HMF) was converted into several biofuel additives such as alkoxymethylfurans (AMFs) and 2,5-bis(alkoxymethyl)furans (BAMFs) through two-step sequential hydrogenation and etherification reactions. In the first step, zinc-iron magnetic nanocatalyst supported on activated carbon ($ZnO\text{-}Fe_3O_4$/AC) was prepared for the selective hydrogenation of HMF into BHMF and 5-MFA via Meerwein-Ponndorf-Verley (MPV) reaction in three different hydrogen donor alcohols (ethanol, 1-propanol, and 1-butanol). The important physical properties of the catalyst such as crystallinity, chemical composition, morphology, reduction behavior, and surface area were studied by using several analytical techniques. The effect of hydrogenation parameters such as catalyst concentration, temperature, and time on the selectivity of (BHMF and 5-MFA), and HMF conversion were studied. The best hydrogenation results were obtained with 0.2 mmole HMF and 100 mg of catalyst at 200 °C for 12 h. In the second step, three commercial Brønsted acid catalysts were used to convert the hydrogenated products into alkoxymethylfurans (AMFs) and 2,5-bis(alkoxymethyl)furans (BAMFs). At the optimum etherification conditions (65 °C and 10 h), a spectrum of mono-, di-, and tri- ether compounds were obtained. The hydrogenation catalyst ($ZnO\text{-}Fe_3O_4$/AC) was recycled and used for five times without a remarkable reduction in its catalytic activity.

1. Introduction

The world's continuous dependence on the three major conventional fossil energy sources (petroleum, coal, and natural gas) leads to the emergence critical environmental issues like the greenhouse effect and the exhaustion of fossil fuels. Consequently, there is a growing concern to use renewable resources as starting feedstock for the production of value-added fuels and chemicals. Biomass is the most appropriate renewable carbon source for biofuels and an alternative for conventional fossil fuels [1–5]. 5-Hydroxymethylfurfural (HMF) is one of the main reaction products along with furfural (FF), levulinic acid (LA), γ-valerolactone, glycerol, sorbitol, xylitol) obtained from the hydrolysis and dehydration of lignocellulosic biomass. HMF valorization processes including etherification [6,7], hydrogenation [8,9], oxidation [10–13], amination [14,15], condensation [16–18], isomerization [18–20] and cyclization reactions [21,22] have a major importance in the development of biorefinery processes. This is due to its role as a unique platform molecule to prepare numerous high value added energy products such as 2,5-dimethylfuran (DMF), ethyl levulinate (EL), γ-valerolactone (GVL), alkoxymethylfurans (AMFs) and 2,5-bis(alkoxymethyl)furans (BAMFs) [3,18,23].

HMF ether products can be utilized as a key raw material in a spectrum of applications including fuel additives, pharmaceuticals, food additives, pesticides, surfactants, spices, paint remover, and rubber modifiers [24,25]. In order to test furfuryl alkyl ethers as a biodiesel additive, different blending ratios were applied in the heavy duty diesel engines and all tested blending ratios show no significant difference in the engine operation [26]. Among HMF ether products, 2-

* Corresponding author.
E-mail address: e.hassan@msstate.edu (E.B. Hassan).

[1] Mention of trade names or commercial products in this publication is solely for the purpose of providing specific information and does not imply recommendation or endorsement by the U.S. Department of Agriculture. USDA is an equal opportunity provider and employer.

https://doi.org/10.1016/j.fuproc.2020.106672
Received 7 August 2020; Received in revised form 8 October 2020; Accepted 8 November 2020
Available online 24 November 2020

alkoxymethylfuran [27], 2-alkoxymethyltetrahydrofuran, and 2,5-bis (alkoxymethyl)tetrahydrofuran [28] were also tested as potential biodiesel candidates.

Taking into consideration the advantages and high value of furfuryl alkyl ethers in multiple applications, it is quite attractive to study the conversion of lignocellulosic biomass-derived HMF into furfuryl alkyl ethers. Till now, the etherification reactions of HMF usually produce either the monoether or the dimer derivative [6,29,30]. In general, furfuryl alkyl ethers preparation can be done through three methods. The first method involves halogenation of furanic alcohols followed by etherification in the presence of aliphatic alcohols, however, this method is less economic because of using the mole equivalent of halogenated agents [31]. The second method involves obtaining 5-ethoxymethylfurfural (EMF) by using chloromethylfurfural as an intermediate in the presence of Brønsted acid catalyst such as Ar-SO_3H-SBA-15 [32]. Utilizing strong Brønsted acid forms ethyl levulinate which is major drawback of this method [33]. The third method, which is considered the most common method for the production of furfuryl alkyl ethers, involves immediate etherification of furan alcoholic group with aliphatic alcohols in the presence of Brønsted acid catalyst.

To prepare 2,5-bis(alkoxymethyl)furan biofuel additives, two reaction steps are required. First is the reduction of HMF to 2,5-bis(hydroxymethyl)furan (BHMF). This is followed by etherification of both hydroxy groups of BHMF with alcohol in the presence of Brønsted acidic catalyst. Prior studies indicated a variety of catalysts such as transition-metal catalysts [34], Brønsted acids [35], Lewis acids [36], and thiourea organocatalyst [37] can catalyze the etherification reaction of furanic alcoholic groups. Achieving high yield of furfuryl ether derivatives is the main challenge facing scientists because most of the previous studies have proceeded in low yield due to the formation of byproducts such as levulinic acid, humin or the reductive homocoupling of the aldehyde components [38]. Han et al. reported a versatile method for the production of potential biodiesels (BAMFs) with more than 70% yield by applying two-step sequential reactions with Ru(OH)$_x$/ZrO_2 catalyst and Amberlyst-15 in various alcohol solvents in the presence of external hydrogen gas [39]. Balakrishnan et al. reported that one pot reductive etherification of HMF with of PtSn/Al_2O_3, and amberlyst-15 co-catalyst in the presence of external hydrogen produced 64% and 47% of 2,5-bis (ethoxymethyl)furan, and 2,5-bis(butoxymethyl)furan by using ethanol and n-butanol, respectively [40]. Gruter et al. also reported that 75% of 2,5-bis(ethoxymethyl)furan can be achieved from the continuous hydrogenation of HMF to 2,5-bis(hydroxymethyl)furan (BHMF) over Pt/C catalyst and etherification in ethanol at 348 K without external hydrogen [41]. Mu et al. obtained 70% yield of 2,5-bis(methoxymethyl) furan (BMMF) by performing the reductive etherification of HMF in a two-step method using Cu/SiO_2 and HZSM-5 co-catalyst system [42]. Li et al. performed the reduction etherification of HMF to (BMMF) using Co-400 catalyst at 140 °C under 2 MPa pressure of external hydrogen and achieved 98.5% yield [3]. Solid acid catalysts such as Sn-Beta and Zr-Beta were also used for the reductive etherification of HMF to BMMF. The substrate concentration and catalyst acidity were the two main factors determining the yield of the etherified products [43].

Currently, conversion of HMF into furfuryl ether is commonly achieved by using a combination of both hydrogenation and acid catalysts in the system. It has been reported that Meerwein-Ponndorf-Verley transfer hydrogenation (MPV) reduction technique using hydrogen donor alcohols, is a promising approach substitutes the dangerous gaseous for hydrogenation of biomass-derived aldehydes due to its selectivity towards the reduction of carbonyl group to hydroxyl group [44,45]. The bimetallic catalysts showed a substantial improvement in the catalytic selectivity, stability, and activity comparing to the monometallic counterparts due to the synergetic effects of the two metals [46–50]. In addition, introducing iron metal in the bimetallic catalyst produces highly abundant, cost-effective, superior magnetic material which make it easy to recover from the chemical reaction by applying an external magnet [47–49,51]. Considering the attractive properties of magnetic bimetallic catalysts, iron-zinc oxides bimetallic catalyst was prepared in this study for the transfer hydrogenation system with three different alcohols. After completing the hydrogenation reaction, the catalyst was removed by a magnet and the etherification reactions were performed by using three different types of Brønsted acids to produce a range of furfuryl ethers. The magnetically recoverable bimetallic nanocatalyst (ZnO-Fe_3O_4/AC) was characterized by XRD, H_2-TPR, ICP-OES, XPS, HRTEM-EDX, and N_2 adsorption-desorption isothermal analyses (BET and BJH). The parameters affecting furfuryl ethers yield including catalyst concentration, alcohol type, time and temperature were optimized.

2. Experimental

2.1. Materials

Zinc (II) nitrate trihydrate (technical grade, 98%), iron (III) nitrate nonahydrate (ACS reagent, ≥98%), 5-methylfurfuryl alcohol (99%), 5-methylfurfural (99%), ethanol (200 proof), and anhydrous sodium hydroxide pellets (≥98%) were purchased from Millipore-Sigma Industrial Corporation. 2,5-bis(hydroxymethyl)furan (BHMF, 98% GC) and 5-hydroxymethylfurfural (HMF, 98%) were purchased from AK Scientific. 1-Butanol (99+%, for spectroscopy), 2,5-dimethylfuran (DMF, 99%), and amberlite IR120 H resin were obtained from Acros organics. 1-Propanol (ACS, 99.5+%), and dowex 50WX2 50–100(H) were obtained from Alfa Aesar. Amberlyst 16 wet was purchased from Fluka analytical. High purity water (17.8 megohm-cm) was used in all experiments. All chemical reagents were used as received without further purification.

2.2. ZnO-Fe_3O_4/AC catalyst preparation

Precipitation-deposition method was used to fabricate Zn-Fe bimetallic catalyst supported on activated carbon (AC) according to the method described in our previous work [45]. Similarly, 1 g of activated carbon was dispersed in deionized water (50 mL) and sonicated for 30 min. The catalyst metallic composition created based on the ratio (1:1:2) of zinc, iron, and activated carbon, respectively. A weight of 2.3 g of Zn $(NO_3)_2.6H_2O$ and 3.7 g $Fe_2(NO_3)_3.9H_2O$ were dispersed in 50 mL water and then sonicated for 10 min. Then, zinc-iron nitrates mixture was gradually added to the activated carbon dispersion dropwise with constant stirring. Next, the metal nitrate mixture was transformed to a metal hydroxide precipitate by the addition of 0.1 M NaOH at 0 °C while the suspension pH was continuously adjusted at 9.5. Subsequently, the suspension was stirred at 20 °C for 1 h, then filtered and washed with deionized water repeatedly until sodium hydroxide was removed from the filtrate. The precipitate was then dried at 80 °C overnight using a vacuum oven and then calcined at 550 °C in air for 5 h. Finally, the calcined catalyst was reduced at 300 °C for 5 h using continuous flow of a gas mixture of 5% H_2 in N_2 (50 mL/min).

2.3. Catalyst characterization

All detailed catalyst characterization methods were described in our previous studies [45,52]. High resolution transmission electron microscope equipped with an energy dispersive X-ray spectroscopy (HRTEM/EDX) images were obtained using JEOL 2100 TEM with LaB6 emitter operated at 200KV. X-ray diffraction (XRD) patterns were recorded with RINT Ultima III XRD (Rigaku Corp., Japan) operating with CuKα1 radiation (λ = 1.54 Å) at 40 KV 44 mA. X-ray photoelectron spectroscopy (XPS) measurements were conducted by a Kratos Axis Ultra X-ray photoelectron spectrometer (Kratos Analytical, Inc., Manchester, UK) using monochromatic Al Kα radiation (1486.6 eV). ICP-OES analyses were performed on a Perkin-Elmer 7000 DV ICP-OES as another tool to determine the catalyst surface chemical composition. The pore size distribution and surface area of the catalyst were measured by a

Quantachrome Autosorb iQ gas sorption analyzer (Anton-Paar, USA). H_2-TPR profiles were performed using 10% H_2 in Ar and a ramp rate of 10 °C/min. Water was removed from the analysis gas by a cold trap maintained at 25 °C and hydrogen consumption was continuously monitored using a thermal conductivity detector (TCD).

2.4. Hydrogenation of HMF

All catalytic experiments were conducted in a 100 mL cylindrical stainless steel reactor (Parr Instruments, USA) connected to external temperature, pressure, and stirring controller [45]. HMF (0.2 mmol) was hydrogenated by employing a group of (ZnO-Fe_3O_4/AC) catalyst weights (from 0 mg to 125 mg), in 15 mL *n*-alcohol in the pressure reactor. The reactor was initially purged with nitrogen (N_2) gas then pressurized to 100 psi. The reactor controller was adjusted at a speed of 500 rpm and heated to the desired temperature (160–200 °C) for different times (6–14 h). At the end of the reaction, an ice-water bath was utilized to cool down the reactor to room temperature, and the catalyst was separated from the reaction mixture by a magnet.

2.5. Etherification of BHMF and 5-MFA

Etherification experiments were conducted in the same hydrogenation medium and on the same reactor after removing ZnO-Fe_3O_4/AC catalyst using an external magnet. Brønsted acid (Amberlyst 16, Amberlyte IR120, or Dowex 50WX2) was then added to the reaction mixture for etherification process. 10 mL of the reaction mixture was mixed with 12.5 mg of the Brønsted acid, then the reactor was sealed, and nitrogen gas was purged through the reactor for 1 min. The reactor was then pressurized into 100 psi with nitrogen gas and the reactor stirrer was adjusted at 500 rpm speed. Etherification reactions were performed at 65 °C for 10 h. At the end of the experiment, the reaction was terminated by immersing the reactor in ice-water bath. Then, the catalyst was separated by filtration, and the etherification products were analyzed by GC/MS.

2.6. Products Analysis

The concentration of HMF, hydrogenation products (BHMF, DMF, 5-MF), and etherification products such as 2,5-bis(ethoxymethyl)furan (BEMF), 5-methylethoxymethylfuran (MEMF), 5-ethoxymethylfurfuryl alcohol (EMFA), and 5-ethoxymethylfuran-diethoxyacetal (EMFDEA), 5-propoxymethylfurfuryl alcohol (PMFA), 2,5-bis(propoxymethyl)furan (BPMF), and 5-propoxymethylfuran-dipropoxyacetal (PMFDPA), 2,5-bis (butoxymethyl)furan (BBMF), 5-butoxymethylfurfuryl alcohol (BMFA), and 5-methybutoxymethylfuran (MBMF) were determined by using GC/MS analysis. A Hewlett Packard 5971 series mass spectrometer connected with fused silica capillary column (VF-Xms, Agilent technologies, Inc.) with dimensions of (30 m × 0.25 mm ID × 0.25 μm film thickness) was used in this study. The initial column temperature (40 °C) was maintained for 1 min, and then, the column temperature was programed at a heating rate of 5 °C/min to 205 °C and hold at 205 °C for 1 min. Both injector and detector temperatures were 280 °C and the carrier gas was Helium of 99.99% purity. The *m/z* values, which represent the fragment ions of the compounds, were recorded for each compound. 1 μL of each sample was injected in the column and the concentration of HMF, BHMF, DMF, 5-MF, and 5-MFA in the mixture were calculated based on standard calibration curve obtained with standard prepared solutions of them. The product's yield, conversion, and selectivity of (HMF, BHMF, DMF, 5-MF, and 5-MFA) were calculated by applying the following equations:

$$\text{Yield}, \% = \left(\frac{\text{Product moles}}{\text{Initial moles of HMF}}\right) \times 100 \quad (1)$$

$$\text{Conversion}, \% = \left(1 - \frac{\text{Moles of unreacted HMF}}{\text{Initial moles of HMF}}\right) \times 100 \quad (2)$$

$$\text{Selectivity}, \% = \left(\frac{\text{Yield}}{\text{Conversion}}\right) \times 100 \quad (3)$$

Furfuryl alkyl ethers components concentrations were measured by GC/MS and displayed as area percent (%).

2.7. Hydrogenation catalyst reusability

At the end of the hydrogenation reaction, an external magnet was applied to separate the magnetic catalyst from the reaction mixture. Then, a mixture of ethanol and DDW was used several times to wash the catalyst in order to remove any impurities followed by reduction under hydrogen for 5 h at 300 °C. The optimum hydrogenation experimental conditions were used during catalyst recyclability.

3. Results and Discussion

3.1. Catalyst characterization

The Catalyst morphological structure was analyzed by using HRTEM as mentioned in Fig. 1. The catalyst elemental analysis was performed by EDX equipped with HRTEM. The quantitative EDX analysis shows the presence of zinc, iron, and carbon in both fresh and recycled catalysts which indicate the functionalization of zinc and iron on the surface of the activated carbon, Fig. 1b, and d. HRTEM images of both fresh and recycled ZnO-Fe_3O_4/AC catalysts clearly confirm the existence of catalyst nanoscale as well as zinc and iron oxides crystals on the surface of activated carbon core, Fig. 1a, and c. HRTEM images show that the average diameter of the catalyst nanoparticles is around 25 nm.

The distribution and oxidation state of the chemical elements on the surface of the prepared catalyst has been proved by performing high-resolution XPS full elemental survey. XPS analysis shown that the catalyst surface consisted mainly of zinc, iron, carbon, and oxygen as mentioned on Fig. 2. The binding energy peaks at 1021.4 eV and 1044 eV correspond to the spin orbit of $Zn^{2+}2p_{3/2}$ and $Zn^{2+}2p_{1/2}$, respectively, which indicates the existence of a divalent oxidation state of ZnO oxide in the prepared catalyst as shown in Fig. 2a, and b. In addition, binding energy peaks at 89 eV and 497.8 eV are attributed to the Zn3p and ZnLMM which are consistent with the existence of Zn as Zinc oxide as presented in Fig. 2c, and d. Fig. 2e shows binding energy peaks at 724.35 eV and 710.81 eV which represent Fe^{3+}2p1/2 and Fe^{3+}2p3/2, in addition to two Fe^{3+} satellite peaks at 732.98 eV and 719.33 eV [45,53]. Also, Fe3p peak was deconvoluted into the Fe^{3+} and Fe^{2+} which present binding energy peaks at 56.5 eV and 55.7 eV that represent Fe^{3+}3p and Fe^{2+}3p as shown in Fig. 2f. Carbon binding energy peak was positioned at 285 eV which attributing to the activated carbon in the catalyst as shown in Fig. 2g. Fig. 2h is stating the location of O1s peak at the lower binding energy of 530.8 eV which is assigned to O^{2-} ions in the ZnO bonding of the wurtzite structure of ZnO [54]. In contrast, the peak located at 531.5 eV was associated with O^{2-} ions in cubic spinel unit cell of Fe_3O_4. XPS peak areas of O1s, Zn3p, and Fe3p were measured and utilized to detect the chemical composition of the catalyst which are 63.99% oxygen, 20.76% zinc, and 15.25% iron lead to a mole ratio of 1.36 (Zn: Fe). ICP-OES analysis provided the elemental composition of the catalyst as follow: 33.3 wt% Zn, 32.6 wt% Fe, and 0.9 wt% Carbon which gives a mole ratio of 1.02 (Zn: Fe).

XRD spectra show well defined diffraction peaks of ZnO, Fe_3O_4, and carbon which were utilized to measure the average crystallite size and crystallinity. Fig. 3a shows XRD patterns of both fresh and recycled ZnO-Fe_3O_4/AC catalyst. From the figure, a set of prominent diffraction peaks of (100, 002, 101, 102, 110, 103, 200, 112, and 201) confirming the existence of ZnO in the catalyst were detected at 2θ of (31.65, 34.65,

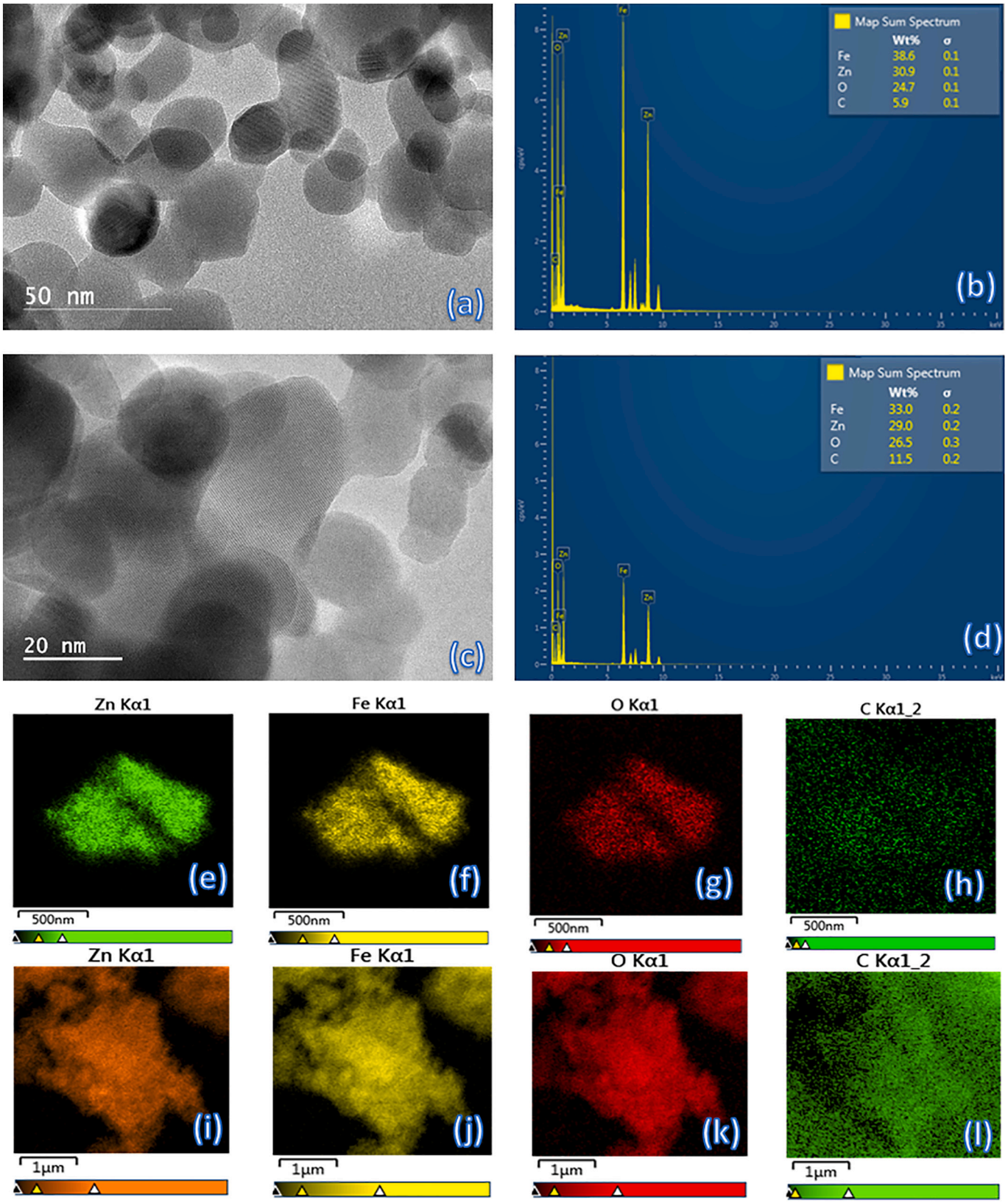

Fig. 1. (a) HRTEM of fresh ZnO-Fe_3O_4/AC catalyst, (b) EDX of fresh ZnO-Fe_3O_4/AC catalyst, (c) HRTEM of recycled ZnO-Fe_3O_4/AC catalyst, (d) EDX of recycled ZnO-Fe_3O_4/AC catalyst, (e-h) EDX mapping images of fresh ZnO-Fe_3O_4/AC, (i-l) EDX mapping images of recycled ZnO-Fe_3O_4/AC.

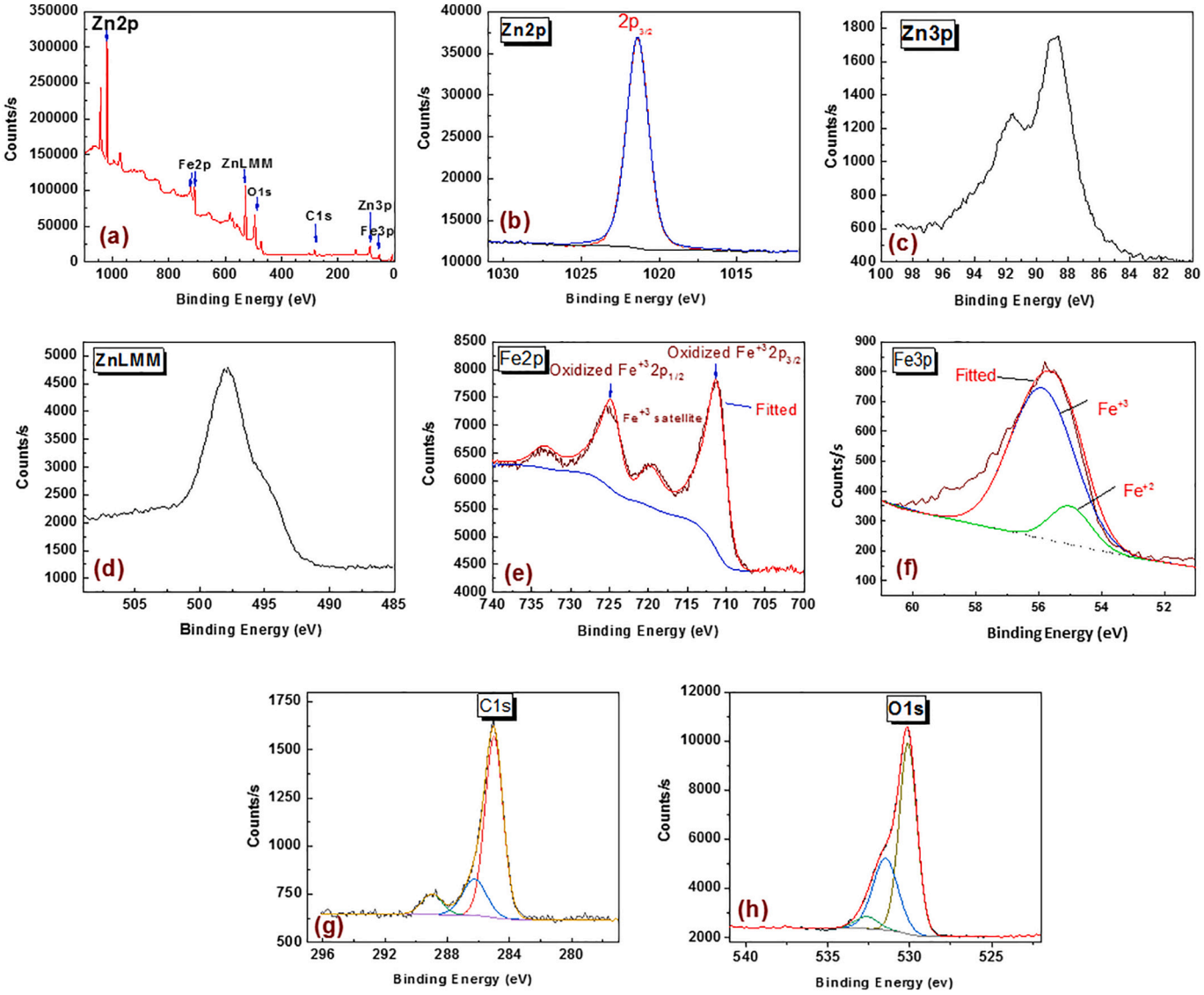

Fig. 2. XPS spectra of ZnO-Fe_3O_4/AC catalyst (a) whole survey scan, (b) Zn2p spectra, (c) Zn3p spectra, (d) Zn LMM spectra, (e) Fe2p spectra, (f) Fe3p spectra, (g) C1s spectra, and (h) O1s spectra.

37.18, 47.25, 56.45, 63.75, 67.73, 68.43, and 69.68 degrees), respectively. The detected peaks are in a good agreement with hexagonal structure of zincite phase reported in JCPDS File Card No.05–0664. In addition, a diffraction peaks of Fe_3O_4 220, 311, 400, 422, 511, 440 and 522 lattice planes are observed at 2θ of 30.2°, 35.6°, 43.2°, 53.9°, 57.3°, 62.9° and 74.7° 2θ were attributed to the cubic spinel unit cell which matches the standard magnetite structure data (JCPDS file no. 19–0629) [55] reflecting the existence of Fe_3O_4 form in the catalyst. Both fresh and recycled catalyst showed the characteristic diffraction peak of graphite at 2θ of 26.4°. The prior XRD results indicate clearly that ZnO, Fe_3O_4, and carbon carrier are the major catalyst constituents. The broad diffraction peaks of XRD pattern indicates the significantly small size of the resulting crystallites. Debye–Scherrer formula ($D = 0.94\lambda / (\beta\cos\theta)$), where λ the X-ray wavelength, β the peak width of half-maximum, and θ is the Bragg diffraction angle, was applied to calculate the ZnO-Fe_3O_4/AC catalyst particle size. From this formula, the average crystallite size of fresh and used catalyst are 26.4 and 24.5 nm respectively, which means that the catalyst crystallite was present after five cycles of hydrogenation reaction with a slight decrease indicating to the stability of the catalyst crystalline structure after hydrogenation reaction cycles. Moreover, the crystallinity of fresh and recycled catalyst was 73.6% and 70.9%, respectively, meaning there was only a small change in the crystallinity after the catalyst was used for five times [56].

H_2-TPR profile for ZnO-Fe_3O_4/AC catalyst was performed to study the interactions between H_2 and reactive sites in the catalyst and the reduction behavior. As shown in Fig. 3b, H_2-TPR profile is a relation of the response signal of TCD versus reduction temperature. In the catalyst H_2-TPR profile, an overlapping reduction peak was observed at temperature range from 350 °C to 660 °C. The overlapping reduction peak consists of two reduction peaks at 499 °C, and 531 °C along with two shoulders at 465 °C, 590 °C which are attributed to the overlapping between the reduction peaks of ZnO, and Fe_3O_4 and traces from Fe_2O_3. The broad peak was Gaussian fitted to four reduction peaks at 465 °C, 499 °C, 531 °C, and 590 °C. The first reduction peak at 465 °C corresponds to reduction of Fe_2O_3 to Fe_3O_4 which a little shifted to the higher temperature region due to the overlapping with ZnO, and Fe_3O_4 peaks. The subsequent reduction peak at 499 °C can be attributed to the reduction of ZnO to Zn(0) [57,58]. The following reduction peak at 531 °C represents the reduction of Fe_3O_4 to FeO [58,59]. Finally, the higher reduction peak observed at 590 °C could be related to the reduction of FeO to Fe(0) [58,59]. The H_2-TPR data are consistent with the catalysts being a mixture of zinc and iron oxides.

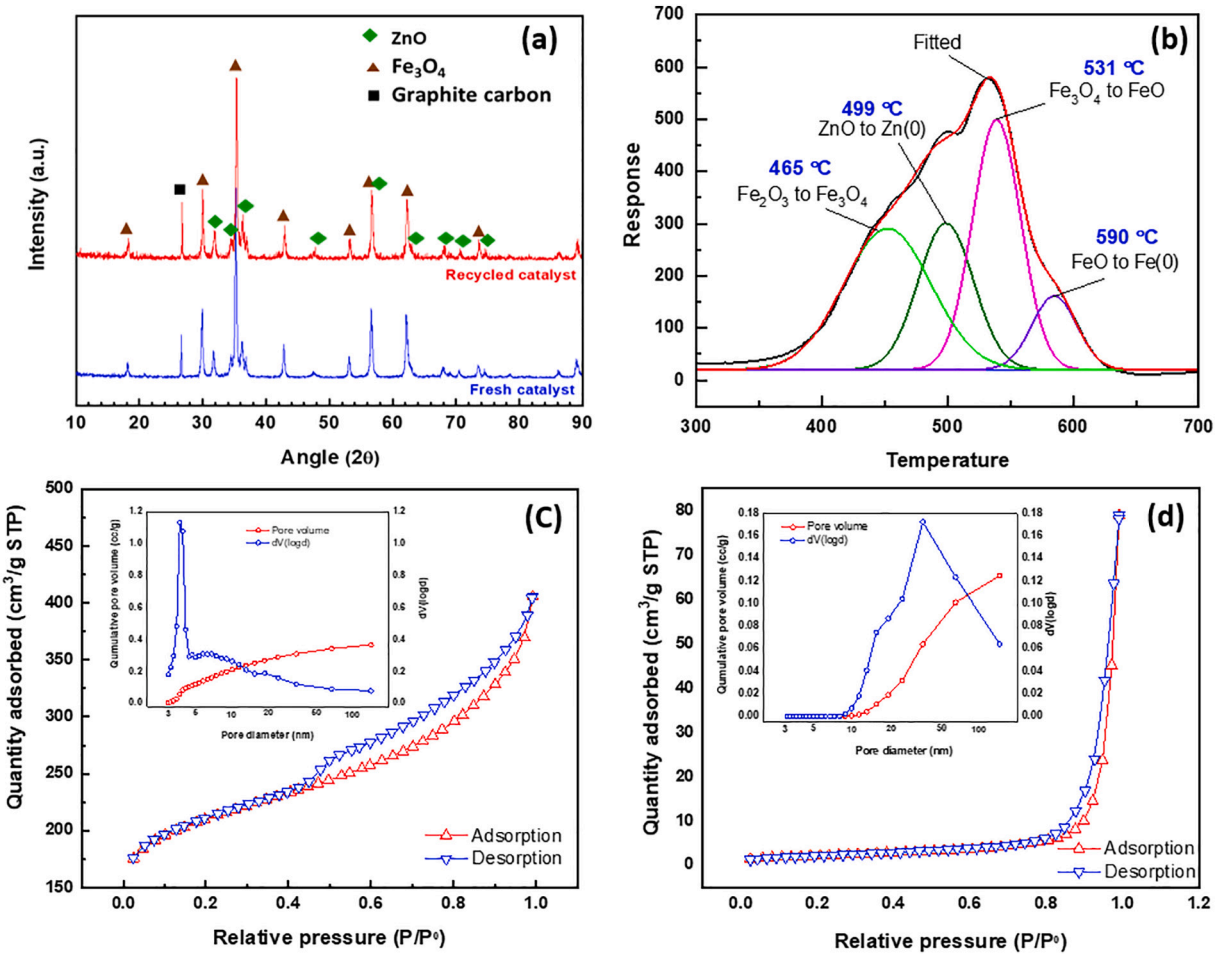

Fig. 3. (a) XRD spectra of fresh and recycled ZnO-Fe_3O_4/AC catalyst, (b) Temperature programing reduction (H_2-TPR) curve of ZnO-Fe_3O_4/AC catalyst, (c) and (d) Nitrogen adsorption-desorption isotherms at -−196 °C with the corresponding average pore size distribution of activated carbon and ZnO-Fe_3O_4/AC catalyst.

The catalyst texture structure including pore size distribution, and surface area was obtained by nitrogen adsorption-desorption isotherm. BET and BJH methods were applied to measure pore size distribution and surface area for both catalyst and activated carbon carrier. As shown in Fig. 3c, the adsorption-desorption isotherm of activated carbon support material behaved as a typical type IV adsorption isotherm with hysteresis loop which means a mesoporous structure for the carrier with a surface area 685 m^2/g, total pore volume 0.627 cc/g, and average pore diameter 3.6 nm. The adsorption-desorption isotherm of ZnO-Fe_3O_4/AC catalyst shows type III adsorption isotherm which means a non-porous or macro-porous structure with decreasing surface area, pore volume, and average pore size to 7.5 m^2/g, 0.12 cc/g, and 35.9 nm, respectively as mentioned in Fig. 3d. The reduction of the surface area and the pore volume is due to the combustion of the activated carbon during the preparation of the catalyst.

3.2. Reactions kinetics of proposed reaction mechanism pathways

The proposed reaction mechanism for the conversion of HMF through both hydrogenation and etherification steps is explained in Scheme 1. The mechanism explains the conversion pathways of HMF converted to BHMF,5-MF, 5-MFA and DMF through hydrogen transfer catalytic reduction using three alcohols in presence of ZnO-Fe_3O_4/AC magnetic nanocatalyst followed by etherification reactions of the hydrogenated products by commercial Brønsted acid catalysts forming furfuryl alkyl ether compounds. Three different reaction temperatures (453.15, 463.15, and 473.15 K) were used to identify the kinetic parameters of the hydrogenation reactions. During all experiments of the kinetic measurements, a high concentration of the hydrogen transfer alcohol (1-propanol,20 mL, 0.267 mol) comparing to substrate concentration (HMF, 0.01 mmol) was used in order to presume a constant concentration of alcohol. Therefore, we have applied pseudo-first order law model to determine the kinetic rate constants and activation energies for each compound of the hydrogenation reactions. The kinetic equations and parameters evaluations were performed typically like the previous published study [45], using OriginPro 2020b software with the application of Levenberg-Marquardt algorithm. Fig. 4 displays the experimental data curve fitting at the applied temperature. The Arrhenius equation was applied to measure the activation energies of the hydrogenation products, and Arrhenius plot can be seen in Fig. S8. Reaction rate constants and activation energies of the hydrogenation products at the applied temperatures with the fittingness error functions are displayed in Tables 1 and 2. To test the goodness of the curves fitting, some fittingness error functions which reflect the error distribution between the experimental and calculated data such as residual sum of squares (RSS), coefficient of determination (COD), reduced Chi-square (χ^2), root mean square of the error, or the Standard Deviation (Root-MSE (SD)) has been measured by the following equations.

$$RSS = \sum_{i=1}^{n} \left(C_{exp.} - C_{calc.}\right)^2 \quad (4)$$

Where n is the number of experimental points, while $C_{exp.}$ and $C_{calc.}$ are the experimental and calculated concentrations (mol L^{-1}).

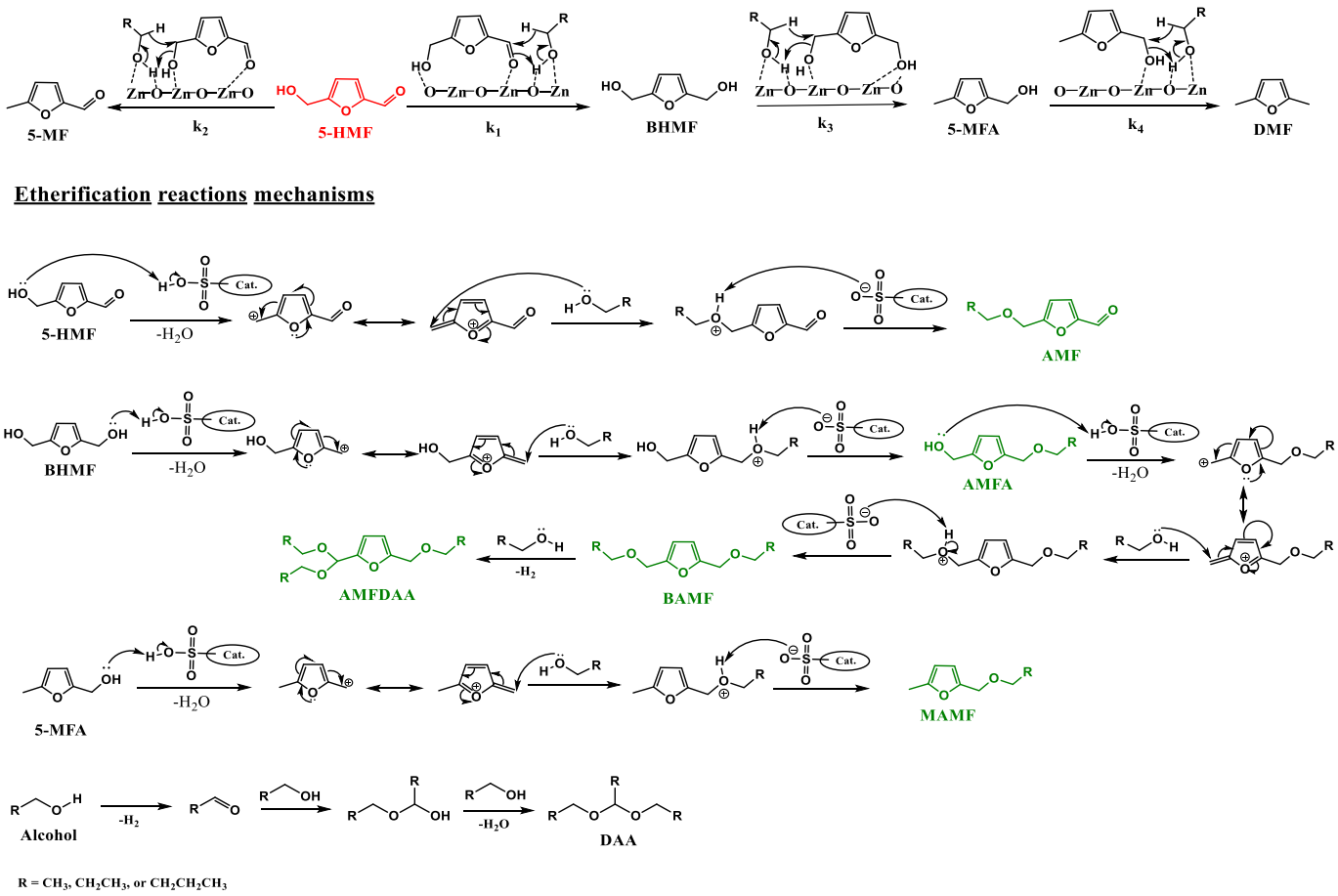

Scheme 1. Proposed reaction mechanism for conversion of HMF to furfuryl alkyl ethers.

$$TSS = \sum_{i=1}^{n} \left(C_{exp.} - C_{mean}\right)^2 \quad (5)$$

Where *TSS* is the total sum of squares, and C_{mean} is the mean experimental concentration (mol L^{-1}).

$$R - square\ (COD) = 1 - \frac{RSS}{TSS} \quad (6)$$

$$Reduced\ Chi - Sqr\ (\chi 2) = \frac{RSS}{df_{Error}} \quad (7)$$

$$Root - MSE\ (SD) = \sqrt{RSS/df_{Error}} \quad (8)$$

Where df_{Error} is the degree of freedom error which equal the number of experimental points (n) divided by the number of parameters (p). From kinetic results, pseudo first-order reaction hypothesis was favored due to the excellent linearity of the correlation coefficient (R^2) at all applied temperatures. By looking to Table 1, the reaction rate constant for the hydrogenation of HMF to form BHMF (k_1) is notably higher than the rate constants for the hydrogenation of HMF to form 5-MF (k_2) in all reaction temperatures which explains the high yield of BHMF. Likewise, the reaction rate constant for the hydrogenation of 5-MFA to form DMF (k_4) is remarkably larger than the rate constants for the hydrogenation of BHMF to form 5-HMA (k_3). Subsequently, the hydrogenation reaction rate of forming 5-MFA is the rate-limiting step for producing DMF. Therefore, obtaining DMF as a main hydrogenation product requires performing the reaction at higher temperature for longer times to make the reaction more selective towards DMF rather than BHMF. By looking to Table 2, the activation energy for the formation of BHMF (39.0 kJ mol^{-1}) was the lowest activation energy obtained in this study. The statistics error methods were used as indicator to test if the fitted regression curve is in good fit with the experimental data or not. From statistics results of the reaction rate constants and activation energies, RSS, (χ^2), and SD are too small values closing to zero, while COD value is closing to 1 which means a good model fit with the experimental data. Both hydrogenation and etherification products were identified by GC/MS analysis as shown in the supporting information Figs. S1-S7.

3.3. Effect of catalyst loading on the hydrogenation of HMF

In this study, three different hydrogen donor alcohols including ethanol, 1-propanol, and 1-butanol were investigated to produce a range of hydrogenated furanic intermediates for the preparation of various furfuryl ethers. As mentioned in the prior studies, the type of the hydrogen donor used has a significant influence on the catalytic transfer hydrogenation reaction of HMF to BHMF [45]. The three alcohols used in this study were chosen according to the previous reports which indicated their high activities as a hydrogen donors [60]. All three alcohols showed higher ability in the hydrogen transfer experiments of HMF to BHMF. Fig. 5 exhibits the effect of ZnO-Fe_3O_4/AC catalyst loading on the transfer hydrogenation reaction of HMF in ethanol, 1-propanol, and 1-butanol solvents. Different amounts of catalyst ranging from 0 to 125 mg were applied while the temperature, time, HMF concentration, and alcohol amount were kept constant in all experiments. The variation in both product selectivity and HMF conversion were determined and represented in Fig. 5a. In the absence of

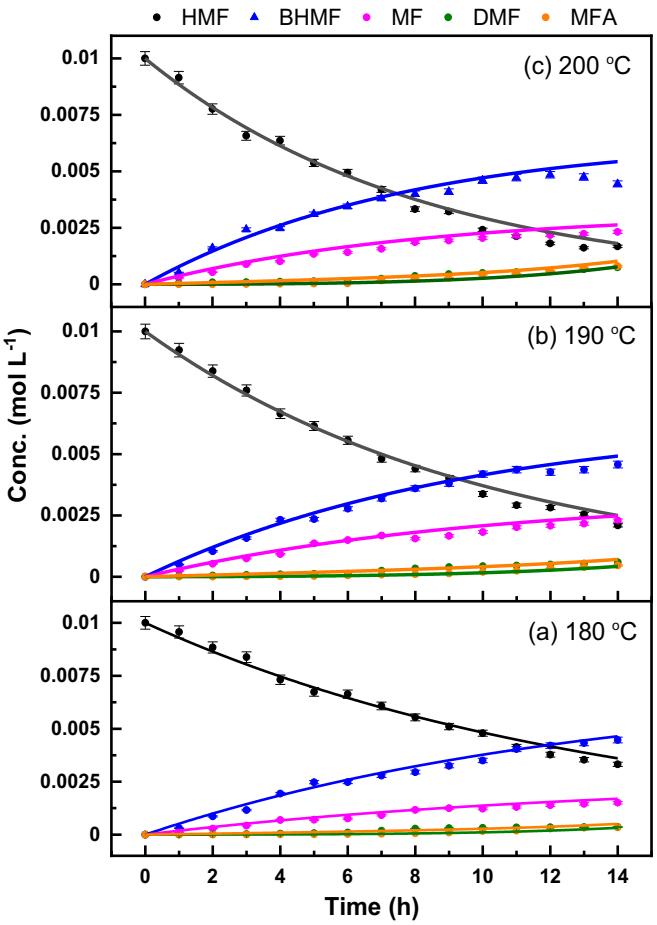

Fig. 4. Model (solid line) and experimental data (markers) of HMF and hydrogenation products (BHMF, MF, DMF, and MFA) over ZnO-Fe_3O_4/AC catalyst at different temperatures 180, 190, and 200 °C.

catalyst, very high selectivity of BHMF (87.9%) was obtained at very low HMF conversion (6.6%) indicating the importance of catalyst for the transfer hydrogenation process. The yield of MF byproduct was relatively small ~12%. Increasing the amount of catalyst to 25 mg led to an obvious increase in the conversion of HMF to ~81% with a relative decrease in the selectivity of the total hydrogenation products (BHMF and MFA) to ~74.6%. Although MFA is not the targeted compound, however, it can be used for the formation of alkoxy ethers in presence of acids. The yield of MF byproduct was relatively increased to ~25.4%. Increasing the amount of catalyst to 100 mg resulted in gradual increase in the total selectivity of (BHMF and MFA) to 80.2% and HMF conversion to 99.7%. Further increase in the catalyst load to 125 mg, slightly decreased the total selectivity of (BHMF and MFA) to 79.2% with 100% conversion. Therefore, 100 mg catalyst load was considered to be the optimal in the case of ethanol as the donor solvent. Fig. 5b shows the effect of catalyst loadings in the hydrogenation products selectivity and HMF conversion utilizing 1-propanol as hydrogen donor. Similar to ethanol, at 100 mg catalyst load, the highest total selectivity of hydrogenation products (BHMF and MFA), HMF conversion, and MF byproduct were 67.6%, 93.2, and 25.4%, respectively. The formation of DMF as a byproduct in this system was also observed. Further increase in the catalyst amount to 125 mg slightly decreased the total selectivity of (BHMF and MFA) to 65.2%. HMF conversion was slightly increased to 95.4% due to the over hydrogenation of BHMF forming several byproduct compounds such as DMF and MF. Fig. 5c shows the effect of catalyst loadings in the hydrogenation products selectivity and HMF conversion utilizing 1-butanol as hydrogen donor. Similarly to the results obtained with ethanol and 1-propanol, at 100 mg catalyst, the highest selectivity of hydrogenation products (74.6%) at 90.2% HMF conversion were achieved. As a result, 100 mg catalyst loading was considered the best catalyst load for 1-propanol and 1-butanol solvents as well.

3.4. Effect of reaction temperature on the hydrogenation of HMF

Previous studies have been reported that time and temperature are the main parameters affecting the hydrogenation reaction of HMF [60]. Moreover, formation of the byproducts such as DMF, and MF are always accompanied with the prolonged reaction time and higher temperatures. Therefore, the effect of the hydrogenation reaction temperature on the products selectivity and HMF conversion was studied in this section. Hydrogenation experiments were performed at fixed catalyst load, time, HMF to alcohol ratio, and various reaction temperatures ranging from 160 °C to 200 °C.

The effect of reaction temperature on the selectivity of the major hydrogenation products (BHMF and MFA), and HMF conversion in ethanol, 1-propanol, and 1-butanol are shown in Fig. 6. In case of ethanol solvent, Fig. 6a, it was found that the lowest reaction temperature (160 °C) favors the formation of BHMF as major hydrogenation product with selectivity 78.8%. Elevating the reaction temperature from 170 to 200 °C led to the formation of MFA as another hydrogenation product. The selectivity of hydrogenation products (BHMF and MFA), and MF byproduct at 200 °C were increased to (80.4%, 19.6%, respectively). Also, HMF conversion was gradually increased from 35.2% at 160 °C to 99.7% at 200 °C. The above results clearly indicate that the higher reaction temperature has a substantial effect on the products selectivity and HMF conversion. Figs. (6b, and c) shows a similar trend for the effect of temperature on the hydrogenation process with 1-propanol and 1-butanol solvents. The highest selectivity of hydrogenation products, byproducts, and HMF conversion were also observed at 200 °C. Accordingly, it was concluded in this study that 200 °C was the optimum hydrogenation reaction temperature for this system.

Table 2
Calculated reaction activation energies with error analysis for the hydrogenation of HMF over ZnO-Fe_3O_4/AC catalyst.

Temp, °C	Activation energy EA (kJ mol^{-1})	Residual sum of squares $\times 10^{-4}$	Root-MSE (SD) $\times 10^{-3}$	R^2 (COD)
K_1 (s^{-1})	39.00	0.68	8.22	0.999
K_2 (s^{-1})	63.30	29.50	54.35	0.988
K_3 (s^{-1})	53.82	15.50	39.42	0.991
K_4 (s^{-1})	28.18	3.90	19.75	0.992

Table 1
Calculated reaction rate constants with error analysis for the hydrogenation of HMF over ZnO-Fe_3O_4/AC catalyst.

Temp, °C	Rate constants, (s^{-1})				Reduced Chi-Sqr (χ^2) $\times 10^{-8}$	Residual sum of squares $\times 10^{-6}$	Root-MSE (SD) $\times 10^{-4}$	R^2 (COD)
	k_1	k_2	k_3	k_4				
180	0.0536	0.0193	0.0015	0.1449	2.26	1.61	1.50	0.996
190	0.0663	0.0296	0.0021	0.1663	2.56	1.82	1.60	0.995
200	0.0830	0.0392	0.0027	0.1989	6.37	4.52	2.52	0.987

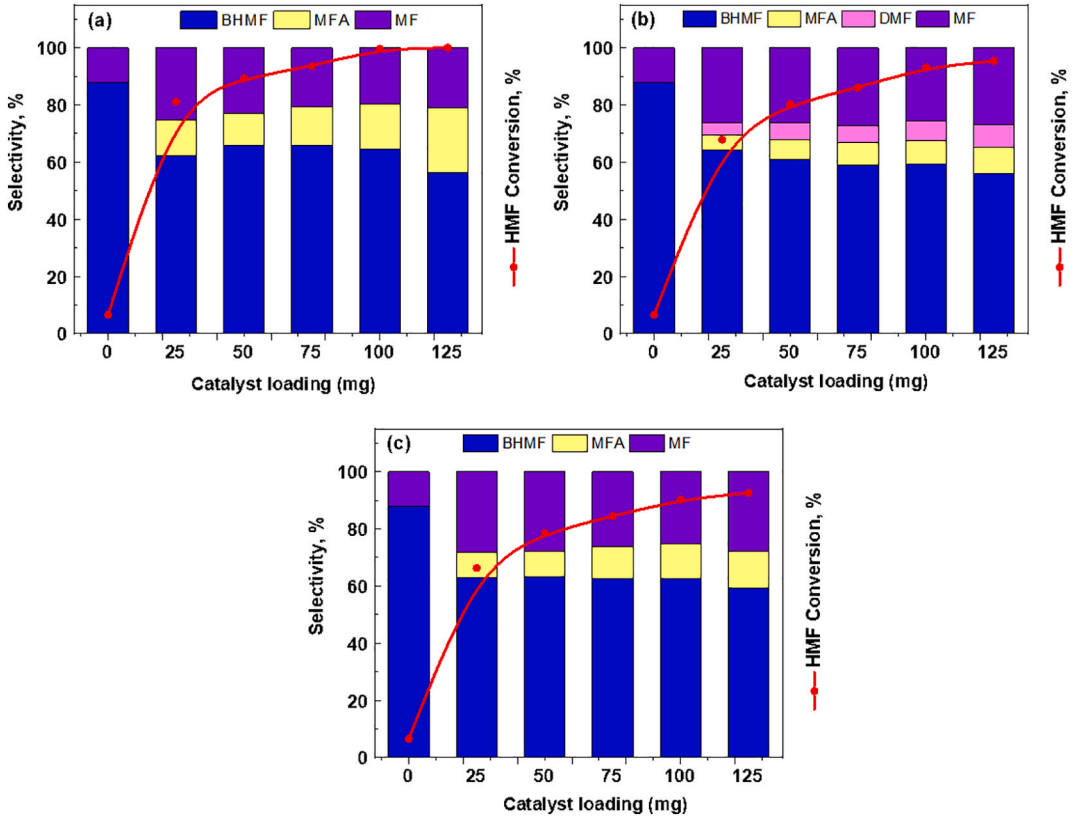

Fig. 5. Effect of ZnO-Fe_3O_4/AC catalyst concentration on the hydrogenation of HMF with different alcohols, (a) Ethanol; (b) 1-propanol; (c) 1-butanol (Hydrogenation conditions are: 0.2 mmol HMF,12 h, and 200 °C).

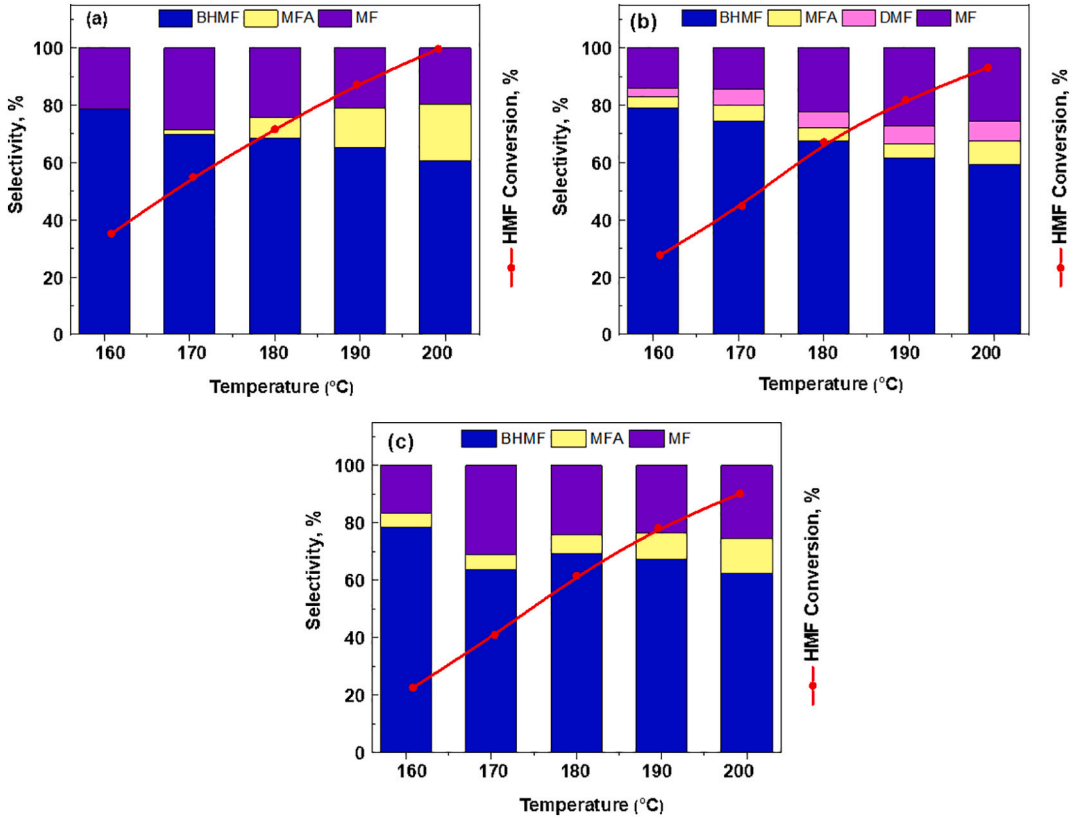

Fig. 6. Effect of reaction temperature on the hydrogenation of HMF with different alcohols, (a) Ethanol; (b) 1-propanol; (c) 1-butanol (Hydrogenation conditions are: 0.2 mmol HMF, 100 mg catalyst, and 12 h).

3.5. Effect of reaction time on the hydrogenation of HMF

Fig. 7 presents the effect of reaction time on the hydrogenation reaction of HMF with the three alcohols. It is very clear from the figure that the hydrogenation process proceeds with a very similar selectivity and HMF conversion trends in all alcohols used. Increasing the reaction time from 6 h to 14 h had a significant effect on both selectivity and HMF conversion. After 6 h reaction time, HMF conversion values were extremely low with all alcohols indicating not enough time to achieve complete hydrogenation process. The selectivity towards the major hydrogenation products that can form ethers with acids (BHMF and MFA) were 84.1% with ethanol, 87.3% with 1-propanol, and 70.2 with1-butanol solvent (Fig. 7a, b, and c). Similarly, HMF conversion to all hydrogenation products (BHMF, MFA, and MF) was also low with all alcohols (46.9% with ethanol, 39.0% with 1-propanol, and 34.6% with 1-butanol). Expanding the reaction time to 12 h led to a remarkable increase in both selectivity and HMF conversion. The selectivity towards (BHMF and MFA) were 80.2% with ethanol, 67.6% with 1-propanol, and 74.6% with 1-butanol solvent. Lower selectivity in case of 1-propanol due to the formation of DMF (6.5%). Also, HMF conversion reached maximum (99.7% with ethanol, 93.2% with 1-propanol, and 90.3% with 1-butanol) after 12 h. In the case of 1-propanol and 1-butanol solvents, further increase in the reaction time to 14 h slightly increased HMF conversion, but this led primarily to over hydrogenation of BHMF to form MF. Therefore, it is not desirable to extend the reaction time over 12 h. Based on the above results, it was concluded that 12 h is the optimum hydrogenation time for the subsequent etherification experiments.

3.6. Etherification of hydrogenation products to biofuel additives

Fig. 8a displays the etherification products in ethanol using Amberlyst 16, Amberlyte IR120, and Dowex 50WX2 Brønsted acids. Besides the targeted biofuel component of 2,5-bis(ethoxymethyl)furan (BEMF), other products which could be considered as potential biofuel additives such as 5-methylethoxymethylfuran (MEMF), 5-ethoxymethylfurfuryl alcohol (EMFA), and 5-ethoxymethylfuran-diethoxyacetal (EMFDEA) were also obtained. Etherification with Amberlyst 16 as acid catalyst produced 64.8% of BEMF, 17.8% of EMFA, and 7.4% of MEMF in addition to byproducts such as 8.6% MF, and 1.6% 5-ethoxymethylfurfural (EMF). When Amberlyte IR120 was used as catalyst, the percentage of BEMF and MEMF were slightly decreased to 60.1%, and 7%, respectively. On the other hand, the percentages of EMFA and byproducts were increased to 19.4% and 9.6%, respectively. The behavior of Dowex 50WX2 as Brønsted acid catalyst was different than Amberlyst 16 and Amberlyte IR120. Applying Dowex 50WX2 produced 18% of the high molecular weight biofuel component (EMFDEA), in addition to 61.8% of BEMF, 4.1% of MEMF, and 6.1% of MF. The total biofuel components produced after using Amberlyst 16, Amberlyte IR120, and Dowex 50WX2 Brønsted acids in ethanol were 90.0%, 86.6%, and 84.0%, respectively.

When 1- propanol was used as solvent, a new series of higher molecular weight ethers where produced after etherification step. 5-Propoxymethylfurfuryl alcohol (PMFA) monoether, 2,5-bis (propoxymethyl)furan (BPMF) diether, and 5-propoxymethylfuran-dipropoxyacetal (PMFDPA) triether were produced with all tested Brønsted acids as presented in Fig. 8b. Etherification using Amberlyst 16 catalyst produced 53.5% of BPMF, 15.5% of PMFA, 3.2% of PMFDPA, 5.2% of MPMF, 15.5% of MF, and 7% of 5-propoxymethylfurfural (PMF). The percentages of both MF and PMFA byproducts increased to 17% and 19.2% when Amberlyte IR120 was used as Brønsted acid catalyst. The increase in the amount of byproducts with Amberlyte IR120 was accompanied with a decrease in the amount of BPMF diether to 46.6% and PMFDPA triether to 2.1%. When Dowex 50WX2 was used as catalyst, the percentage of BPMF, PMFDPA, and unknown compounds were increased to 49.2%, 8%, and 12.9%, respectively. On the other

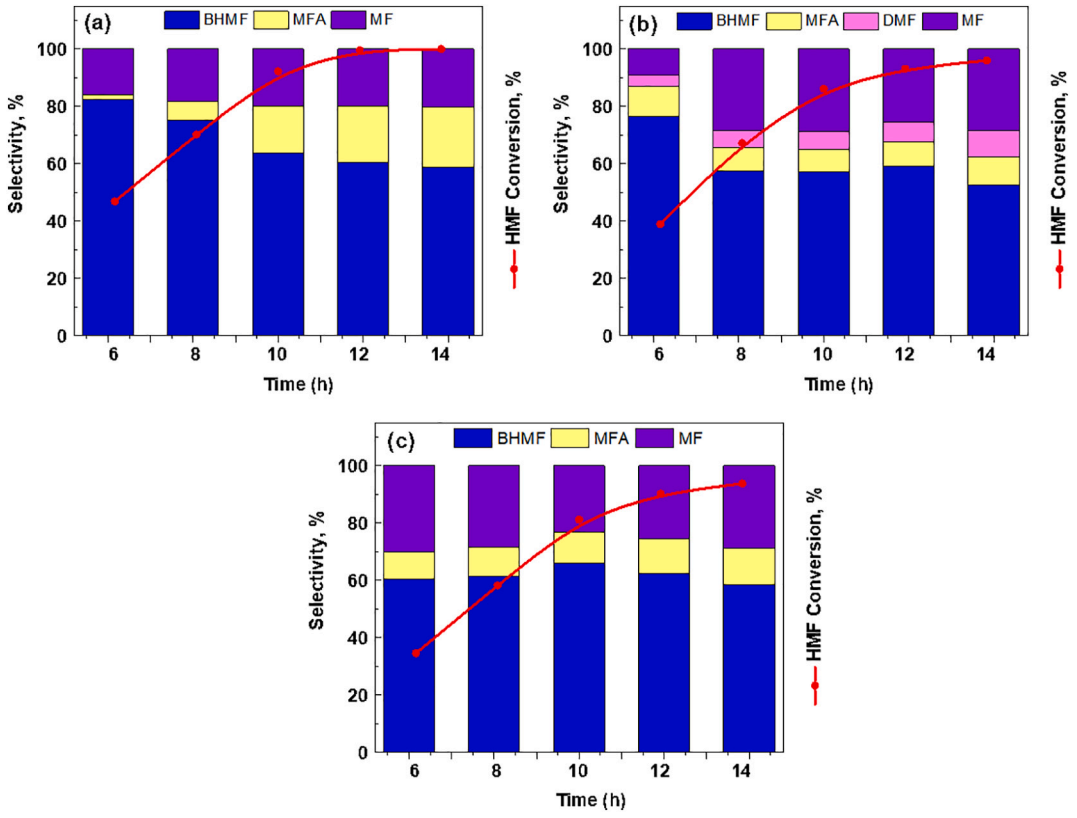

Fig. 7. Effect of reaction time on the hydrogenation of HMF with different alcohols, (a) Ethanol; (b) 1-propanol; (c) 1-butanol (Hydrogenation conditions are: 0.2 mmol HMF, 100 mg catalyst, and 200 °C).

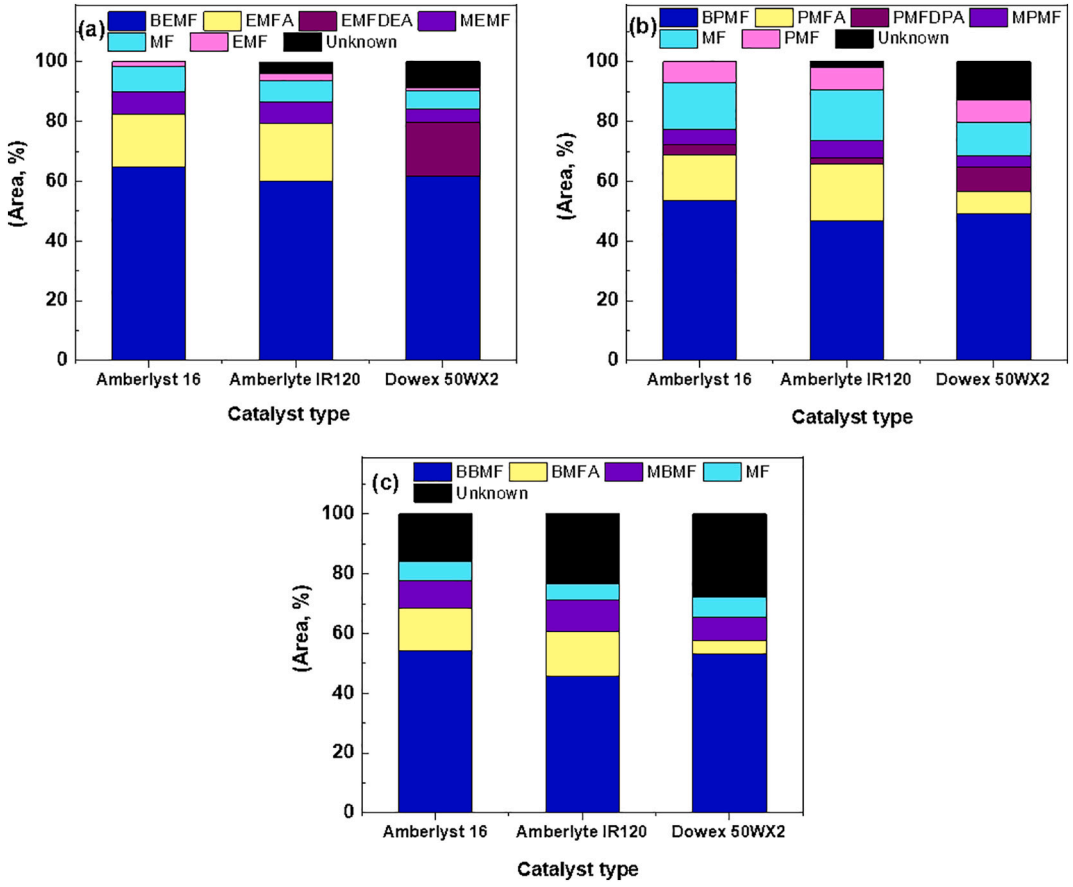

Fig. 8. Etherification products obtained from the hydrogenated HMF with different alcohols, (a) Ethanol; (b) 1-propanol; (c) 1-butanol (Etherification conditions are: 10 mL of reaction mixture, 12.5 mg catalyst, 10 h, and 65 °C).

hand, the percentage of PMFA, MPMF, PMF, and MF were decreased to 7.4%, 3.8%, 7.2%, and 11.4%, respectively. The total etherified products produced with 1-propanol solvent were 77.4% with Amberlyst 16 catalyst, 73.6% with Amberlyte IR120, and 68.4% with Dowex 50WX2 catalyst.

The highest molecular weight etherified products were produced with 1-butanol solvent are displayed in Fig. 8c. Amberlyst 16 formed 54.3% of 2,5-bis(butoxymethyl)furan (BBMF), 14.1% of 5-butoxymethylfurfuryl alcohol (BMFA), and 9.18% of 5-methybutoxymethylfuran (MBMF) along with 6.48% of MF, and 15.85% of unknown products. The percentage of BMFA, MBMF, and the unknown products were increased to 15.0%, 10.5%, and 23.3%, respectively. On contrary, the percentage of both BBMF and MF were decreased to 45.57%, and 5.59%, respectively. By examining Dowex 50WX2 as catalyst, the percentages of both BBMF and the unknown products were increased to 53.2% and 27.7%, while BMFA, MBMF, and MF percentages were reduced to 4.3%, 7.7%, and 7.0%, respectively. The total etherified products produced with 1-butanol solvent was 77.7% with Amberlyst 16 catalyst, 71.1% with Amberlyte IR120, and 65.3% with Dowex 50WX2 catalyst. In conclusion, the yield of our obtained etherification products prepared in ethanol, 1-propanol, or 1-butanol were higher than the yields of etherification products reported in the previous literatures [39–43].

3.7. Catalyst reusability

Stability of catalyst has a great effect in reducing the cost of HMF conversion to biofuel additives in large scale production. As a result of using commercial catalysts in the etherification step, the stability of the hydrogenation catalyst (ZnO-Fe_3O_4/AC) was studied and the reusability results are shown in Fig. 9. 1-Propanol was chosen as solvent to test the catalyst recyclability through five recycling tests. Twenty five percent of the optimum catalyst load (25 mg) was used in this study to be sure that there is no excessive catalyst compared with the amount of HMF. Through five recycling runs, the catalyst retained its unique catalytic reactivity as the selectivity towards BHMF was slightly changed and the conversion of HMF was also slightly decreased from 67.9% to 64.1%. These results indicating clearly that the leaching of the catalyst surface active sites was minimal during the hydrogenation of HMF to BHMF.

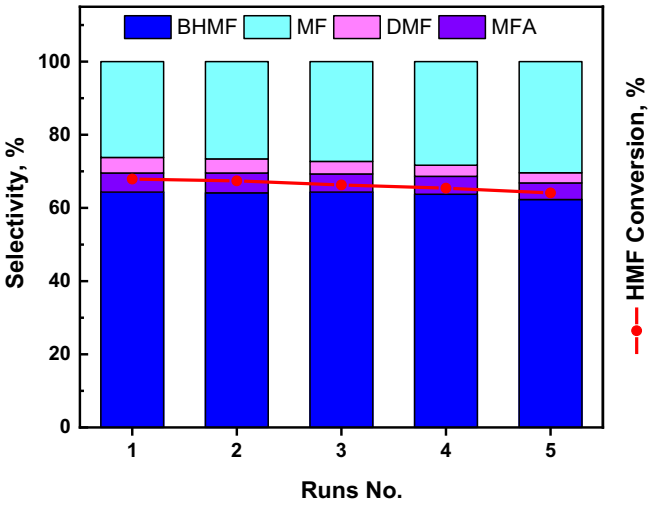

Fig. 9. ZnO-Fe_3O_4/AC catalyst reusability (Hydrogenation conditions are: 0.2 mmol HMF, 25 mg catalyst, 1-propanol, 12 h, and 200 °C).

Finally, the catalyst could be used for five cycles without apparent decrease in its catalytic activity.

4. Conclusion

Two-step sequential reaction process including hydrogenation followed by etherification were developed to produce a spectrum of alkoxymethylfurans (AMFs) and 2,5-bis(alkoxymethyl)furans (BAMFs) from HMF. A magnetically recoverable cost-effective bimetallic nanocatalyst (ZnO-Fe_3O_4/AC) was prepared and used for the hydrogenation step in three hydrogen donor alcohols. Etherification step was performed by using different Brønsted acid catalysts such as Amberlyst 16, Amberlyte IR120, and Dowex 50WX2. Hydrogenation reaction parameters such as catalyst load, temperature, and time significantly affected the selectivity of the hydrogenation products and HMF conversion. Features of the hydrogenation catalyst obtained using XRD, H_2-TPR, ICP-OES, XPS, HRTEM, TGA, and surface texture measurements, were consistent with a mixed metal oxide of uniform structure. At the optimum conditions of hydrogenation step, the selectivity towards (BHMF and MFA) were 80.2% with ethanol, 67.6% with 1-propanol, and 74.6% with 1-butanol. Also, HMF conversion was 99.7% with ethanol, 93.2% with 1-propanol, and 90.3% with 1-butanol. In the etherification step, the highest biofuel yields were achieved with ethanol solvent using Amberlyst 16, Amberlyte IR120, and Dowex 50WX2 heterogenous Brønsted acids were 90.0%, 86.6%, and 84.0%, respectively. The highest molecular weight etherified products were obtained with 1-propanol and 1-butanol solvents. Kinetic studies revealed that the hydrogenation of HMF proceeds mainly through a pseudo-first-order kinetic model and the activation energy of BHMF formation was much lower than the activation energy of 5-MF formation. Also, the hydrogenation reaction rate of 5-MFA formation was the rate-limiting step to produce DMF. Lastly, the prepared hydrogenation catalyst (ZnO-Fe_3O_4/AC) could be used five times without an obvious loss in its catalytic activity.

CRediT authorship contribution statement

Islam Elsayed: Conceptualization, Methodology, Writing - original draft. **Michael A. Jackson:** Methodology, Writing - review & editing. **El Barbary Hassan:** Supervision, Conceptualization, Writing - review & editing, Project administration.

Declaration of Competing Interest

There are no conflicts to declare.

Acknowledgment

“The authors wish to acknowledge the support of U.S. Department of Agriculture (USDA), Research, Education, and Economics (REE), Agriculture Research Service (ARS), Administrative and Financial Management (AFM), Financial Management and Accounting Division (FMAD) Grants and Agreements Management Branch (GAMB), under Agreement No. 58-0202-6-001. Any opinions, findings, conclusion, or recommendations expressed in this publication are those of the author(s) and do not necessarily reflect the view of the U.S. Department of Agriculture”.

XPS data were collected at the Frederick Seitz Materials Research Laboratory Central Research Facilities at the University of Illinois Urbana-Champaign.

Appendix A. Supplementary data

Supplementary data to this article can be found online at https://doi.org/10.1016/j.fuproc.2020.106672.

References

[1] M. Besson, P. Gallezot, C. Pinel, Conversion of biomass into chemicals over Metal catalysts, Chem. Rev. 114 (2014) 1827–1870, https://doi.org/10.1021/cr4002269.
[2] M.J. Gilkey, B. Xu, Heterogeneous catalytic transfer hydrogenation as an effective pathway in biomass upgrading, ACS Catal. 6 (2016) 1420–1436, https://doi.org/10.1021/acscatal.5b02171.
[3] X.-L. Li, K. Zhang, S.-Y. Chen, C. Li, F. Li, H.-J. Xu, Y. Fu, A cobalt catalyst for reductive etherification of 5-hydroxymethyl-furfural to 2,5-bis(methoxymethyl) furan under mild conditions, Green Chem. 20 (2018) 1095–1105, https://doi.org/10.1039/C7GC03072J.
[4] Y. Nakagawa, S. Liu, M. Tamura, K. Tomishige, Catalytic total hydrodeoxygenation of biomass-derived polyfunctionalized substrates to alkanes, ChemSusChem 8 (2015) 1114–1132, https://doi.org/10.1002/cssc.201403330.
[5] H. Nguyen, N. Xiao, S. Daniels, N. Marcella, J. Timoshenko, A. Frenkel, D. G. Vlachos, Role of Lewis and Brønsted acidity in metal chloride catalysis in organic media: reductive etherification of furanics, ACS Catal. 7 (2017) 7363–7370, https://doi.org/10.1021/acscatal.7b02348.
[6] H. Li, S. Saravanamurugan, S. Yang, A. Riisager, Direct transformation of carbohydrates to the biofuel 5-ethoxymethylfurfural by solid acid catalysts, Green Chem. 18 (2016) 726–734, https://doi.org/10.1039/C5GC01043H.
[7] G.A. Kraus, T. Guney, A direct synthesis of 5-alkoxymethylfurfural ethers from fructose via sulfonic acid-functionalized ionic liquids, Green Chem. 14 (2012) 1593–1596, https://doi.org/10.1039/C2GC35175G.
[8] X. Tang, J. Wei, N. Ding, Y. Sun, X. Zeng, L. Hu, S. Liu, T. Lei, L. Lin, Chemoselective hydrogenation of biomass derived 5-hydroxymethylfurfural to diols: Key intermediates for sustainable chemicals, materials and fuels, Renew. Sust. Energ. Rev. 77 (2017) 287–296, https://doi.org/10.1016/j.rser.2017.04.013.
[9] T.-W. Tzeng, C.-Y. Lin, C.-W. Pao, J.-L. Chen, R.J.G. Nuguid, P.-W. Chung, Understanding catalytic hydrogenolysis of 5-hydroxymethylfurfural (HMF) to 2,5-dimethylfuran (DMF) using carbon supported Ru catalysts, Fuel Process. Technol. 199 (2020) 106225, https://doi.org/10.1016/j.fuproc.2019.106225.
[10] G. Yi, S.P. Teong, Y. Zhang, Base-free conversion of 5-hydroxymethylfurfural to 2,5-furandicarboxylic acid over a Ru/C catalyst, Green Chem. 18 (2016) 979–983, https://doi.org/10.1039/C5GC01584G.
[11] C. Zhou, W. Shi, X. Wan, Y. Meng, Y. Yao, Z. Guo, Y. Dai, C. Wang, Y. Yang, Oxidation of 5-hydroxymethylfurfural over a magnetic iron oxide decorated rGO supporting Pt nanocatalyst, Catal. Today 330 (2019) 92–100, https://doi.org/10.1016/j.cattod.2018.05.037.
[12] Q. Li, H. Wang, Z. Tian, Y. Weng, C. Wang, J. Ma, C. Zhu, W. Li, Q. Liu, L. Ma, Selective oxidation of 5-hydroxymethylfurfural to 2,5-furandicarboxylic acid over au/CeO_2 catalysts: the morphology effect of CeO_2, Catal Sci Technol. 9 (2019) 1570–1580, https://doi.org/10.1039/C9CY00211A.
[13] H. Xia, S. Xu, H. Hu, J. An, C. Li, Efficient conversion of 5-hydroxymethylfurfural to high-value chemicals by chemo- and bio-catalysis, RSC Adv. 8 (2018) 30875–30886, https://doi.org/10.1039/C8RA05308A.
[14] W. Chen, Y. Sun, J. Du, Z. Si, X. Tang, X. Zeng, L. Lin, S. Liu, T. Lei, Preparation of 5-(Aminomethyl)-2-furanmethanol by direct reductive amination of 5-Hydroxymethylfurfural with aqueous ammonia over the Ni/SBA-15 catalyst, J. Chem. Technol. Biotechnol. 93 (2018) 3028–3034, https://doi.org/10.1002/jctb.5661.
[15] X. Wang, W. Chen, Z. Li, X. Zeng, X. Tang, Y. Sun, T. Lei, L. Lin, Synthesis of bis (amino)furans from biomass based 5-hydroxymethyl furfural, J Energy Chem. 27 (2018) 209–214, https://doi.org/10.1016/j.jechem.2017.06.015.
[16] R. Lee, J.R. Vanderveen, P. Champagne, P.G. Jessop, CO_2-Catalysed aldol condensation of 5-hydroxymethylfurfural and acetone to a jet fuel precursor, Green Chem. 18 (2016) 5118–5121, https://doi.org/10.1039/C6GC01697A.
[17] R.S. Malkar, H. Daly, C. Hardacre, G.D. Yadav, Aldol condensation of 5-hydroxymethylfurfural to fuel precursor over novel aluminum exchanged-DTP@ZIF-8, ACS Sustain. Chem. Eng. 7 (2019) 16215–16224, https://doi.org/10.1021/acssuschemeng.9b02939.
[18] W. Fan, C. Verrier, Y. Queneau, F. Popowycz, 5-Hydroxymethylfurfural (HMF) in organic synthesis: a Review of its recent applications towards fine chemicals, Curr. Org. Synth. 16 (2019) 583–614, https://doi.org/10.2174/1570179416666190412164738.
[19] Q. Deng, X. Wen, P. Zhang, Pd/Cu-MOF as a highly efficient catalyst for synthesis of cyclopentanone compounds from biomass-derived furanic aldehydes, Catal. Commun. 126 (2019) 5–9, https://doi.org/10.1016/j.catcom.2019.04.008.
[20] S. Zhang, H. Ma, Y. Sun, Y. Luo, X. Liu, M. Zhang, J. Gao, J. Xu, Catalytic selective hydrogenation and rearrangement of 5-hydroxymethylfurfural to 3-hydroxymethyl-cyclopentone over a bimetallic nickel–copper catalyst in water, Green Chem. 21 (2019) 1702–1709, https://doi.org/10.1039/C8GC04009E.
[21] L. Hu, L. Lin, Z. Wu, S. Zhou, S. Liu, Recent advances in catalytic transformation of biomass-derived 5-hydroxymethylfurfural into the innovative fuels and chemicals, Renew. Sust. Energ. Rev. 74 (2017) 230–257, https://doi.org/10.1016/j.rser.2017.02.042.
[22] R.F.A. Gomes, J.A.S. Coelho, C.A.M. Afonso, Direct conversion of activated 5-hydroxymethylfurfural into δ-lactone-fused cyclopentenones, ChemSusChem 12 (2019) 420–425, https://doi.org/10.1002/cssc.201802537.
[23] Q.-S. Kong, X.-L. Li, H.-J. Xu, Y. Fu, Conversion of 5-hydroxymethylfurfural to chemicals: a review of catalytic routes and product applications, Fuel Process. Technol. 209 (2020) 106528, https://doi.org/10.1016/j.fuproc.2020.106528.
[24] K.S. Arias, M.J. Climent, A. Corma, S. Iborra, Biomass-derived chemicals: Synthesis of biodegradable surfactant ether molecules from hydroxymethylfurfural, ChemSusChem 7 (2014) 210–220, https://doi.org/10.1002/cssc.201300531.

[25] M. Mascal, E.B. Nikitin, High-yield conversion of plant biomass into the key value-added feedstocks 5-(hydroxymethyl)furfural, levulinic acid, and levulinic esters via 5-(chloromethyl)furfural, Green Chem. 12 (2010) 370–373, https://doi.org/10.1039/B918922J.
[26] E. de Jong, T. Vijlbrief, R. Hijkoop, G.-J.M. Gruter, J.C. van der Waal, Promising results with YXY Diesel components in an ESC test cycle using a PACCAR Diesel engine, Biomass Bioenergy 36 (2012) 151–159, https://doi.org/10.1016/j.biombioe.2011.10.034.
[27] M. Paniagua, J.A. Melero, J. Iglesias, G. Morales, B. Hernández, C. López-Aguado, Catalytic upgrading of furfuryl alcohol to bio-products: Catalysts screening and kinetic analysis, Appl Catal, A 537 (2017) 74–82, https://doi.org/10.1016/j.apcata.2017.03.004.
[28] J.D. Stenger-Smith, L. Baldwin, A. Chafin, P.A. Goodman, Synthesis and Characterization of bis(Tetrahydrofurfuryl) Ether, ChemistryOpen 5 (2016) 297–300, 10.1002%2Fopen.201600013.
[29] S. Alipour, H. Omidvarborna, D.-S. Kim, A review on synthesis of alkoxymethyl furfural, a biofuel candidate, Renew. Sust. Energ. Rev. 71 (2017) 908–926, https://doi.org/10.1016/j.rser.2016.12.118.
[30] J. Wang, Z. Zhang, S. Jin, X. Shen, Efficient conversion of carbohydrates into 5-hydroxylmethylfurfan and 5-ethoxymethylfurfural over sufonic acid-functionalized mesoporous carbon catalyst, Fuel 192 (2017) 102–107, https://doi.org/10.1016/j.fuel.2016.12.027.
[31] J.E. Zanetti, Alpha furfuryl ethers, I, J Am Chem Soc. 49 (1927) 1065–1067, https://doi.org/10.1021/ja01403a028.
[32] P. Lanzafame, D.M. Temi, S. Perathoner, G. Centi, A. Macario, A. Aloise, G. Giordano, Etherification of 5-hydroxymethyl-2-furfural (HMF) with ethanol to biodiesel components using mesoporous solid acidic catalysts, Catal. Today 175 (2011) 435–441, https://doi.org/10.1016/j.cattod.2011.05.008.
[33] G. Morales, M. Paniagua, J.A. Melero, J. Iglesias, Efficient production of 5-ethoxymethylfurfural from fructose by sulfonic mesostructured silica using DMSO as co-solvent, Catal. Today 279 (2017) 305–316, https://doi.org/10.1016/j.cattod.2016.02.016.
[34] K. Iwanami, K. Yano, T. Oriyama, Iron(III) Chloride-catalyzed reductive etherification of carbonyl compounds with alcohols, Chem. Lett. 36 (2007) 38–39, https://doi.org/10.1246/cl.2007.38.
[35] M.P. Doyle, D.J. DeBruyn, D.A. Kooistra, Silane reductions in acidic media I. Reduction of aldehydes and ketones in alcoholic acidic media. General synthesis of ethers, J Am Chem Soc. 94 (1972) 3659–3661, https://doi.org/10.1021/ja00765a084.
[36] M. Bakos, Á. Gyömöre, A. Domján, T. Soós, Auto-tandem catalysis with frustrated Lewis pairs for reductive etherification of aldehydes and ketones, Angew. Chem. Int. Ed. 56 (2017) 5217–5221, https://doi.org/10.1002/anie.201700231.
[37] M.B. Sassaman, G.K. Surya Prakash, G.A. Olah, P. Donald, K.B. Loker, Ionic hydrogenation with organosilanes under acid-free conditions. synthesis of ethers, alkoxysilanes, thioethers, and cyclic ethers via rganosilyl iodide and triflate catalyzed reductions of carbonyl compounds and their derivatives, Tetrahedron 44 (1988) 3771–3780, https://doi.org/10.1016/S0040-4020(01)86635-7.
[38] C. Zhao, C.A. Sojdak, W. Myint, D. Seidel, Reductive etherification via anion-binding catalysis, J. Am. Chem. Soc. 139 (2017) 10224–10227, https://doi.org/10.1021/jacs.7b05832.
[39] J. Han, Y.-H. Kim, B.Y. Jung, S.H. Hwang, J. Jegal, J.W. Kim, Y.-S. Lee, Highly selective catalytic hydrogenation and etherification of 5-hydroxymethyl-2-furaldehyde to 2,5-bis(alkoxymethyl)furans for potential biodiesel production, Synlett 28 (2017) 2299–2302, https://doi.org/10.1055/s-0036-1589076.
[40] M. Balakrishnan, E.R. Sacia, A.T. Bell, Etherification and reductive etherification of 5-(hydroxymethyl)furfural: 5-(alkoxymethyl)furfurals and 2,5-bis(alkoxymethyl) furans as potential bio-diesel candidates, Green Chem. 14 (2012) 1626–1634, https://doi.org/10.1039/C2GC35102A.
[41] G.J.M. Gruter, US8231693B2, (2012).
[42] Q. Cao, W. Liang, J. Guan, L. Wang, Q. Qu, X. Zhang, X. Wang, X. Mu, Catalytic synthesis of 2,5-bis-methoxymethylfuran: a promising cetane number improver for diesel, Applied Catalysis A 481 (2014) 49–53, https://doi.org/10.1016/j.apcata.2014.05.003.
[43] H. Li, Z. Fang, R.L. Smith, S. Yang, Efficient valorization of biomass to biofuels with bifunctional solid catalytic materials, Prog. Energy Combust. Sci. 55 (2016) 98–194, https://doi.org/10.1016/j.pecs.2016.04.004.
[44] J. Song, B. Zhou, H. Zhou, L. Wu, Q. Meng, Z. Liu, B. Han, Porous zirconium–phytic acid hybrid: a highly efficient catalyst for meerwein–ponndorf–verley reductions, Angew. Chem. Int. Ed. 54 (2015) 9399–9403, https://doi.org/10.1002/anie.201504001.
[45] I. Elsayed, M.A. Jackson, E.B. Hassan, Hydrogen-free catalytic reduction of biomass-derived 5-hydroxymethylfurfural into 2,5-bis(hydroxymethyl)furan using copper–iron oxides bimetallic nanocatalyst, ACS Sustain. Chem. Eng. 8 (2020) 1774–1785, https://doi.org/10.1021/acssuschemeng.9b05575.
[46] G.D. Yadav, Y.S. Lawate, Hydrogenation of styrene oxide to 2-phenyl ethanol over polyurea microencapsulated mono- and bimetallic nanocatalysts: activity, selectivity, and kinetic modeling, Ind. Eng. Chem. Res. 52 (2013) 4027–4039, https://doi.org/10.1021/ie302587j.
[47] W. Tang, J. Li, X. Jin, J. Sun, J. Huang, R. Li, Magnetically recyclable Fe@Pd/C as a highly active catalyst for Suzuki coupling reaction in aqueous solution, Catal. Commun. 43 (2014) 75–78, https://doi.org/10.1016/j.catcom.2013.09.001.
[48] S.C. Patankar, G.D. Yadav, Cascade engineered synthesis of γ-valerolactone, 1,4-pentanediol, and 2-methyltetrahydrofuran from levulinic acid using pd–cu/zro$_2$catalyst in water as solvent, ACS Sustain. Chem. Eng. 3 (2015) 2619–2630, https://doi.org/10.1021/acssuschemeng.5b00763.
[49] S.C. Patankar, S.K. Dodiya, G.D. Yadav, Cascade engineered synthesis of ethyl benzyl acetoacetate and methyl isobutyl ketone (MIBK) on novel multifunctional catalyst, J. Mol. Catal. A Chem. 409 (2015) 171–182, https://doi.org/10.1016/j.molcata.2015.08.018.
[50] A.D. Talpade, M.S. Tiwari, G.D. Yadav, Selective hydrogenation of bio-based 5-hydroxymethyl furfural to 2,5-dimethylfuran over magnetically separable Fe-Pd/C bimetallic nanocatalyst, Mol Catalysis 465 (2019) 1–15, https://doi.org/10.1016/j.mcat.2018.12.009.
[51] M.S. Tiwari, A.B. Gawade, G.D. Yadav, Magnetically separable sulfated zirconia as highly active acidic catalysts for selective synthesis of ethyl levulinate from furfuryl alcohol, Green Chem. 19 (2017) 963–976.
[52] I. Elsayed, M. Mashaly, F. Eltaweel, M.A. Jackson, E.B. Hassan, Dehydration of glucose to 5-hydroxymethylfurfural by a core-shell Fe_3O_4@SiO_2-SO_3H magnetic nanoparticle catalyst, Fuel 221 (2018) 407–416, https://doi.org/10.1016/j.fuel.2018.02.135.
[53] T. Yamashita, P. Hayes, Analysis of XPS spectra of Fe^{2+} and Fe^{3+} ions in oxide materials, Appl. Surf. Sci. 254 (2008) 2441–2449, https://doi.org/10.1016/j.apsusc.2007.09.063.
[54] R. Sankar Ganesh, M. Navaneethan, G.K. Mani, S. Ponnusamy, K. Tsuchiya, C. Muthamizhchelvan, S. Kawasaki, Y. Hayakawa, Influence of Al doping on the structural, morphological, optical, and gas sensing properties of ZnO nanorods, Journal of Alloys and Compounds 698 (2017) 555–564, https://doi.org/10.1016/j.jallcom.2016.12.187.
[55] G.-Q. Yuan, H.-F. Jiang, C. Lin, S.-J. Liao, Shape- and size-controlled electrochemical synthesis of cupric oxide nanocrystals, J. Cryst. Growth 303 (2007) 400–406, https://doi.org/10.1016/j.jcrysgro.2006.12.047.
[56] U. Holzwarth, N. Gibson, The Scherrer equation versus the 'Debye-Scherrer equation', Nat. Nanotechnol. 6 (2011) 534, https://doi.org/10.1038/nnano.2011.145.
[57] Y. Lv, W. Yao, X. Ma, C. Pan, R. Zong, Y. Zhu, The surface oxygen vacancy induced visible activity and enhanced UV activity of a ZnO_{1-x} photocatalyst, Catalysis Science & Technology 3 (2013) 3136–3146, https://doi.org/10.1039/C3CY00369H.
[58] A. Khan, P.G. Smirniotis, Relationship between temperature-programmed reduction profile and activity of modified ferrite-based catalysts for WGS reaction, J. Mol. Catal. A Chem. 280 (2008) 43–51, https://doi.org/10.1016/j.molcata.2007.10.022.
[59] B. Espro, E. Gumina, F. Paone, Mauriello, Upgrading Lignocellulosic Biomasses: Hydrogenolysis of Platform Derived Molecules Promoted by Heterogeneous Pd-Fe Catalysts, Catalysts 7 (2017) 78, https://doi.org/10.3390/catal7030078.
[60] L. Hu, J. Xu, S. Zhou, A. He, X. Tang, L. Lin, J. Xu, Y. Zhao, Catalytic advances in the production and Application of Biomass-Derived 2,5-Dihydroxymethylfuran, ACS Catal. 8 (2018) 2959–2980, https://doi.org/10.1021/acscatal.7b03530.